Observed and CMIP6 model simulated organic aerosol response to drought in the contiguous United States during summertime

Wei Li[1,2] and Yuxuan Wang[1]

[1]Department of Earth and Atmospheric Sciences, University of Houston, Houston, Texas, USA

[2]Now at Cooperative Institute for Satellite Earth System Studies, George Mason University, Fairfax, Virginia, USA

Corresponding author: Yuxuan Wang (ywang246@central.uh.edu)

Abstract. Drought events have been linked with the enhancements of organic aerosols (OA), but the mechanisms have not been comprehensively understood. This study investigates the relationships between the monthly standardized precipitation–evapotranspiration index (SPEI) and surface OA in the contiguous United States (CONUS) during the summertime from 1998 to 20189. OA under severe drought conditions shows a significant increase in mass concentrations across most of the CONUS relative to non-drought periods with the Pacific Northwest (PNW) and Southeastern United States (SEUS) experiencing the highest average enhancement of 1.79 $\mu g\,m^{-3}$ (112 %) and 0.92 $\mu g\,m^{-3}$ (33 %), respectively. In the SEUS, a linear regression approach between OA and sulfate was used to estimate the epoxydiols-derived secondary organic aerosol (IEPOX SOA), which is the primary driver of the OA enhancements under droughts due to the simultaneous increase in biogenic volatile organic compounds (VOCs; such as isoprene and monoterpene) emissions and sulfate. The rise of sulfate is mainly caused by the reduced wet deposition because of the up to 62% lower precipitation amount. In the PNW, OA enhancements are closely linked to intensified wildfire emissions, which raise OA mass concentrations to be four to eight times higher relative to non-fire conditions. All ten Earth system models participating in the sixth phase of the Coupled Model Intercomparison Project (CMIP6) can capture the slopes between SPEI and OA in the PNW with CESM2-WACCM and GFDL-ESM4 performing the best and worst in predicting the OA enhancement under severe droughts. However, all models significantly underestimate the OA increase in the SEUS with Nor-ESM2-LM and MIRCO6 showing relatively better performance. This study reveals the key drivers of the elevated OA levels under droughts in the CONUS and underscores the deficiencies of current climate models in their predictive capacity for assessing the impact of future droughts on air quality.

1. Introduction

Drought events, marked by prolonged periods of water scarcity and precipitation deficits, have profound impacts on the hydrological cycle, ecosystems, and society (Wilhite et al., 2007). The contiguous United States (CONUS) is especially prone to droughts, and recent years have witnessed an escalation in both the frequency and severity of drought episodes across various regions (Leeper et al., 2022; Strzepek et al., 2010). These drought events are intricately linked to the modifications in atmospheric processes, such as emission, production, transport, and deposition, which can extend beyond the immediate hydrological impacts with far-reaching implications for air

33 quality. Specifically, organic aerosol (OA), a major component of the particulate matter with an aerodynamic

34 diameter less than or equal to 2.5 μm ($PM_{2.5}$), emerges as a critical air quality concern influenced by the complex

35 interactions between drought-induced meteorological conditions and biogeochemical processes.

36 OA can be directly emitted into the atmosphere through combustion activities, such as transportation fuel and

37 biomass burning. This kind of OA is called primary organic aerosol (POA), whereas secondary organic aerosol

38 (SOA) is produced by the oxidation of volatile organic compounds (VOCs). The intricate interplay between drought

39 and OA dynamics involves complex feedback mechanisms. Biogenic isoprene, mainly emitted by terrestrial

40 vegetation, is an important precursor of SOA and is highly sensitive to drought conditions. Both laboratory and field

41 measurements have shown that biogenic emissions of isoprene will increase at the initial stage of drought

42 development primarily due to temperature stimulus but drop eventually under prolonged severe drought limited by

43 soil water availability (Pegoraro et al., 2005; Brilli et al., 2007; Potosnak et al., 2014). The abnormally high

44 temperature and low humidity under droughts can enhance the ~~volatility and~~ oxidation of OA (Maria et al., 2004;

45 Yli-Juuti et al., 2021), while low cloud water content lowers the aqueous SOA formation (Brégonzio-Rozier et al.,

46 2016; Tsui et al., 2019), leading to compensating changes in the mass and hygroscopicity of OA. Aerosols are most

47 effectively removed by wet scavenging, which will be reduced under lower rainfall intensity and frequency (Dawson

48 et al., 2007; Fang et al., 2011). In addition, dry conditions can trigger large and high-intensity wildfires, emitting

49 more POA and VOC precursors into the atmosphere (Ruffault et al., 2018; Taufik et al., 2017). The interactions of

50 these factors underscore the need for a comprehensive understanding of the mechanisms driving variations in OA

51 during drought events.

52 OA, due to its fine particulate nature and diverse chemical composition, exerts significant adverse effects on climate

53 and human health. ~~Exposure to SOA is associated with a 6.5 times higher mortality rate in the CONUS than total~~

54 ~~$PM_{2.5}$ mass~~OA is found to be associated with a higher county-level cardiorespiratory mortality rate than other major

55 $PM_{2.5}$ components, such as sulfate, ammonium, and nitrate (Pye et al., 2021). OA can scatter solar radiation, form

56 cloud condensation nuclei, and affect cloud droplet concentrations, posing big uncertainties on radiative forcing and

57 climate feedback (Carslaw et al., 2013; Lee et al., 2016). The coupled chemistry-climate models and Earth system

58 models (ESMs) are fundamental tools for studying global warming and the accuracy of OA simulations in these

59 models are crucial constraints on their credibility in climate change simulation and projection (Gomez et al., 2023;

60 Thornhill et al., 2021). The Coupled Model Intercomparison Project Phase 6 (CMIP6), containing the new

61 generation of ESMs with interactive aerosol and gas chemistry implemented (Turnock et al., 2020), provides a

62 valuable opportunity to evaluate the simulated OA and its response to drought, which is projected to be more

63 frequent in the future (Cook et al., 2018)

64 Several case studies have focused on the impacts of droughts on the concentrations and speciation of $PM_{2.5}$ in the

65 CONUS by calculating the differences between drought and non-drought years (Wang et al., 2015; Borlina and

66 Rennó, 2017; Zhao et al., 2019). Wang et al. (2015) and Zhao et al. (2019) compared the concentrations of $PM_{2.5}$

67 and its compositions in the southern/southeastern U.S. during the severe drought in the 2011 summertime against the

68 non-drought year of 2010 and 2013, respectively. They show that $PM_{2.5}$ has a respective enhancement of 47% and

69 65% with the largest contribution from the increase of organic carbon (OC) by 119% and 117%. Following OC,

70 sulfate in the southeast US is enhanced by 84% during the 2011 drought relative to 2013. However, fewer studies

71 have carried out long-term analyses, which can help derive a more robust drought-aerosol association than case

72 studies. Wang et al. (2017) performed a 25-year analysis during the growing season (March-October) from 1990 to

73 2014 and found that, on a monthly scale, the overall 17% enhancement of $PM_{2.5}$ in the CONUS is mainly attributed

74 to the increase of OA, sulfate, and dust. Each of these species has a unique spatial pattern in their response to

75 droughts, which warrants a further subregional analysis to reveal the processes causing such spatial distribution

76 discrepancy.

77 In this study, we focus on the changes in OA under droughts over the CONUS during the study period of

78 summertime from 1998 to 2018. Spatial patterns of the responses of OA to droughts will be explored, followed by

79 a regional analysis focusing on the southeastern US (SEUS) and Pacific Northwest (PNW) where the highest

80 responsive rates of OA to droughts are found. The processes responsible for the increase of OA in these regions will

81 be discussed. At last, the observed drought-OA relationships will be used as a process-level metric to evaluate OA

82 simulations in the CMIP6 ESMs, which can shed light on future model development and improve aerosol

83 predictions.

84 **2. Datasets**

85 **2.1 Drought indicator**

86 The one-month gridded Standardized Precipitation-Evapotranspiration Index (SPEI) data from the global SPEI

87 database (https://spei.csic.es/, last access: November 27, 2023) was selected as the drought indicator because of its

88 numerical nature allowing for statistical analysis (e.g., correlation and regression). The SPEI is a multi-scaler index,

89 allowing for the identification and comparison of drought severity through time and space (Vicente-Serrano et al.,

90 2010). Negative values of SPEI are indicative of droughts and vice versa. The dataset has a spatial resolution of 0.5°

91 × 0.5° and a temporal range of 1973-2018. A composite analysis can also be conducted by applying the criteria of

92 SPEI < -1.3 and SPEI > -0.5 to denote severe drought and non-drought conditions, respectively, as suggested by Wang

93 et al. (2017).

94 **2.2 Air quality and meteorological data**

95 To expand the spatial coverage, we created a gridded daily organic carbon (OC) dataset (0.5° × 0.5°) from 1998 to

96 2018 that aggregates site-based observations from the Interagency Monitoring of Protected Visual Environments

97 (IMPROVE) network using the modified inverse distance weighting method as done by Schnell et al. (2014). Data

98 from the IMPROVE sites has been widely used by previous studies to investigate surface particulate matter trends or

99 variations in the CONUS (e.g., Hand et al., 2012). A factor of 2.1 was used to convert OC observations to OA as

100 suggested by other studies (Pye et al., 2017; Schroder et al., 2018). US Environmental Protection Agency Chemical

101 Speciation Network (EPA-CSN) also provides long-term OA data, but the CSN network uses different sampling

102 practices and analytical methods from IMPROVE, which can lead to systematic differences in OA measurements
103 (Hand et al., 2012; Gorham et al., 2021). Thus, we only used the IMPROVE dataset in this study. To reduce the artifact
104 caused by different data completeness (e.g., old sites retired and new sites started), we selected the sites with data
105 records longer than 5 years during the study period for interpolation following Li and Wang (2022). Based on this
106 criterion, there are a total of 175 sites selected for interpolation, ~80% of which have a data record equal to or greater
107 than 15 years, suggesting small temporal uncertainties caused by the spatial interpolation (Figure S1).

108 Sulfate is known to influence the formation of epoxydiols derived secondary organic aerosol (IEPOX SOA), a key
109 component of OA. To explore how this linkage changes with drought, we generated a gridded sulfate dataset following
110 the same method as OC. Monthly sulfate wet depositions with associated precipitation amount and pH were obtained
111 from the National Atmospheric Deposition Program (NADP). There is a total of 53 NADP sites in the SEUS (defined
112 in Section 3.1) with a more than 5-year data record during the study period. We obtained the satellite-based low level
113 (below 700 hPa) cloud cover and liquid water content (LWC) between 2000 to 2018 from the Clouds and the Earth's
114 Radiant Energy System (CERES) monthly Single Scanner Footprint 1° × 1° (SSF1deg) product
115 (https://asdc.larc.nasa.gov/project/CERES/CER_SSF1deg-Month_Terra-MODIS_Edition4A, last access: November
116 28, 2023). To investigate OA changes from wildfire, monthly open fire emissions were from the Global Fire Emission
117 Database version 4 (GFED4) for 1998–2018 (Giglio et al., 2013). The version of GFED4 we used includes the burned
118 area contributions from small fires, which increases the total amount of burned area by 75% relative to its previous
119 version and brings the prescribed burned area estimates into closer agreement with those reported by the National
120 Interagency Fire Center (Randerson et al., 2012). Thus, the prescribed fire burning is partly, if not all, considered in
121 the analysis.

122 **2.3 CMIP6 AerChemMIP models**

123 Ten models from the CMIP6 Aerosol Chemistry Model Intercomparison Project (AerChemMIP) were selected: BCC-
124 ESM1, CESM2-WACCM, CNRM-ESM2-1, EC-Earth3-AerChem, GFDL-ESM4, GISS-E2-1-G, MIROC6, MRI-
125 ESM2-0, NorESM2-LM, and UKESM1-0-LL. They are the only models found by the time of writing with OA and
126 sulfate mass concentration outputs from historical simulations with prescribed sea surface temperature in the
127 AerChemMIP project from 1850 to 2014. No ensemble members were found for the ten models. Various aerosol
128 schemes are used by the models with different treatments for gas phase reactions and secondary aerosol formation.
129 More information and references (Danabasoglu et al., 2020; Dunne et al., 2020; Kelley et al., 2020; van Noije et al.,
130 2021; Séférian et al., 2019; Seland et al., 2020; Senior et al., 2020; Tatebe et al., 2019; Wu et al., 2020; Yukimoto et
131 al., 2019) for each model are listed in Table S1.

132 **3. Results**

133 **3.1 Spatial Distributions of Organic Aerosol Response to Drought**

134 Figure 1a shows the maps of the mean summertime (JJA 1998–2018) surface OA concentrations under non-drought
135 conditions and their changes under severe droughts with the observational sites (dots) overlaid. The associated

136 frequency and OA standard deviation during non-drought and severe drought periods are displayed in Figure S2.

137 The western US states along the Rocky Mountains exhibit the highest severe drought frequency of up to 25%, while

138 wet and normal conditions are more common in the eastern US and southern California with a frequency of more

139 than 80%. -Higher OA concentrations can be found in central California and the eastern US under non-drought

140 conditions, reflecting the average spatial distributions of summertime OA. Under severe droughts, most of the grids

141 and sites display an enhanced OA level with a mean increase of 0.72 µg m^{-3} across all the grids and 0.78 µg m^{-3}

142 across all the sites in the CONUS. Higher enhancements occur in the Pacific Northwest (PNW; 42-50°N, 105-

143 125°W; red box in Figure 1a) and southeast U.S. (SEUS; 25-37°N, 75-100°W; blue box in Figure 1a). In both

144 regions, the overall gridded OA statistical distributions under severe droughts move towards the higher end

145 compared with those under non-drought conditions (Figure 1b), with an increase in the mean value by 1.79 µg m^{-3}

146 (112 %) and 0.92 µg m^{-3} (33 %) across the PNW and SEUS, respectively. Similar results are found using on-site

147 data with a respective increase of mean value by 2.18 µg m^{-3} (118 %) and 1.11 µg m^{-3} (34 %), which indicates the

148 interpolation does not significantly affect the results. OA experienced a downward trend in the SEUS during the last

149 two decades due to the reduction of anthropogenic emissions (Ridley et al., 2018). To verify whether the trend will

150 significantly affect our results in the SEUS, we reproduced Figure 1b in Figure S3a using detrended OA. The

151 detrend is conducted by removing the 7-year moving average from the raw data in the same month of each year

152 following Wang et al. (2017) and Li et al. (2022). OA enhancement under severe droughts is 0.78 µg m^{-3} and 1.02

153 µg m^{-3} for gridded and on-site data, respectively, which is comparable to those values derived from raw OA data in

154 the SEUS area. This indicates that anthropogenic emission changes do not significantly interfere with our analysis

155 and instead natural processes play a more important role in causing the enhancement of OA in the SEUS region.
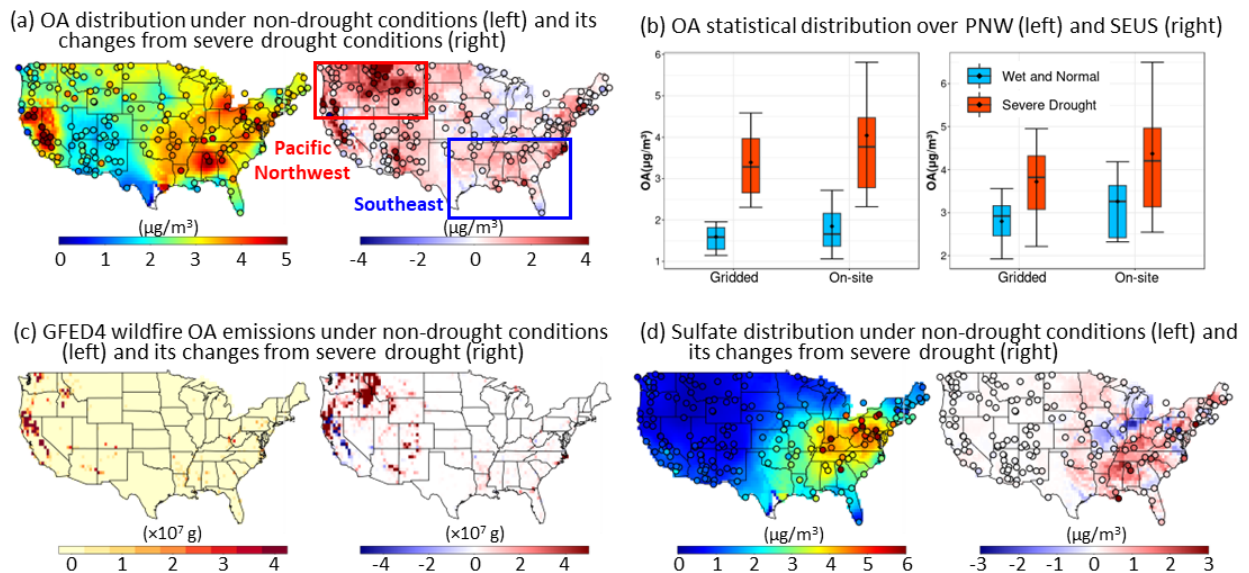
156

157 **Figure 1. (a) Maps of the mean gridded and in situ (dots) OA under non-drought (wet and normal) conditions (left) from**
158 **1998 to 20189 in JJA and its changes from severe drought conditions (right). (b) Comparisons of statistical distributions of**
159 **gridded and on-site OA mass concentrations under severe drought (red boxes) and non-drought (blue boxes) conditions**
160 **over the Pacific Northwest (left) and southeast region (right). (c-d) Same as a, but for OA monthly wildfire emissions from**
161 **GFED4 inventory and sulfate, respectively.**

162 Wildfire, a major source of biomass burning, is one of the biggest contributors to both POA and SOA globally
163 (Hallquist et al., 2009; Gilman et al., 2015; Jen et al., 2019). In the western U.S., OA, as the largest component of
164 PM$_{2.5}$, experiences an upward trend, opposite to the rest of the country, due to the increasingly higher wildfire
165 frequency (Dennison et al., 2014; McClure & Jaffe, 2018; Wang, et al., 2022). Indeed, we found many 'hot spots' of
166 wildfire emissions of OA over the western U.S. under non-drought conditions based on the GFED4 wildfire fire
167 inventory (Figure 1c). Severe droughts can lead to extremely high wildfire OA emissions over the PNW region,
168 which corresponds to the highest OA enhancement and variability as shown in Figure 1a and Figure S2b,
169 respectively. In contrast, the SEUS undergoes a much lower enhancement of wildfire OA emissions under severe
170 droughts. Biogenic secondary organic aerosol (BSOA) is reported to be the major fine aerosol component in the
171 SEUS, accounting for 60%–90% of the total PM$_{2.5}$, due to the abundant isoprene emissions (Zhang et al., 2012;
172 Hidy et al., 2014; Kim et al., 2015). The concentrations of BSOA in the SEUS region strongly depend on ambient
173 sulfate through the reactive update of gas-phase epoxydiols (IEPOX) onto the aqueous acidified surface of sulfate
174 particles (Surratt et al., 2010; Xu et al., 2015; Lopez-Hilfiker et al., 2016; Malm et al., 2017). Interestingly, the
175 highest sulfate increase during drought is found in the SEUS (Figure 1d), presumably due to enhanced gas-phase
176 sulfate production and reduced wet deposition (Wang et al., 2015; Xie et al., 2019). The higher sulfate
177 concentrations during droughts lead to the enhanced formation of IEPOX SOA, which is likely an important factor
178 leading to a higher OA level in the SEUS.
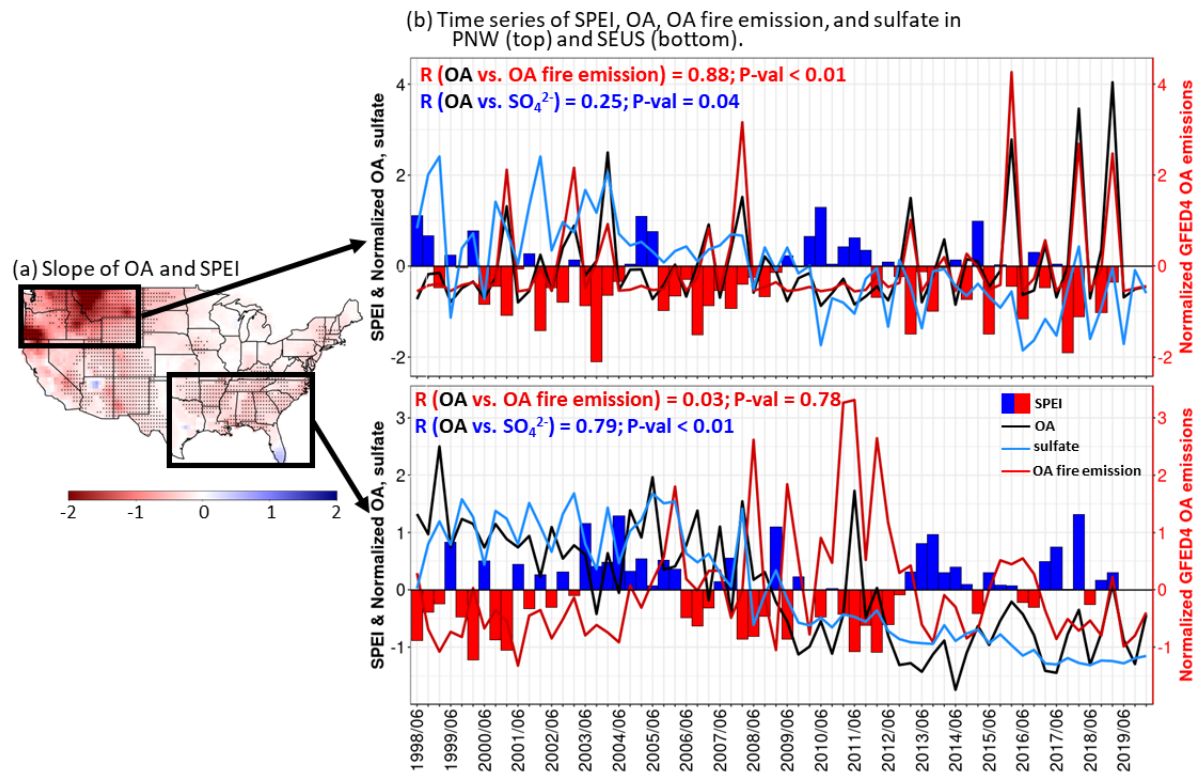
179

180 **Figure 2. (a) Map of the slopes between monthly gridded OA and SPEI. Black dots indicate the slopes with P-vales less than**
181 **0.05. (b) Time series of SPEI (bar), normalized OA (black line), sulfate (blue line), and wildfire OA emissions from GFED4**
182 **inventory (red line; right axis) averaged across the PNW (top) and SEUS (bottom) region. The numbers indicate the**
183 **correlation coefficient (R) and P-value (P-val) between OA and sulfate (blue) and wildfire emissions (red).**

184

Using the numerical drought indicator of SPEI, we calculated the linear slopes between monthly OA and SPEI in

each grid (Figure 2a). Consistent with the composite analysis in Figure 1a, most of the grids show negative slopes

with the highest absolute values of more than 2 µg m^{-3} per unit change of SPEI occurring in the PNW region. It is

noteworthy that ~~Since~~ negative values of SPEI indicate droughts, and thus the negative slopes with SPEI signify an

enhanced OA level over most of the CONUS during drought. We further examined the monthly time series of the

regional mean of SPEI, normalized OA, sulfate, and OA wildfire emissions in the PNW and SEUS (Figure 2b). OA

in the PNW region is strongly correlated with OA emissions from fire with a high correlation coefficient (R) of 0.88.

The extremely high values of OA and OA fire emissions are also concurrent with droughts when SPEI is negative

(red bars). On the contrary, SEUS has a weak correlation between OA and OA fire emissions yet a high association

between OA and sulfate with an R value of 0.79. Wildfire seems only to have high contributions to peak OA values

in extreme drought years, such as in 2011. Based on the correlation coefficients, more than 60% and 70% of the

monthly OA variability can be explained by sulfate and wildfire emissions in the SEUS and PNW regions,

respectively, which deserves an in-depth exploration in the next section.

198

3.2 Regional Analysis in the Pacific Northwest and Southeast US

In this section, we conducted a regional analysis of OA, focusing on OA relationships with sulfate in the SEUS and

with wildfire emissions in the PNW. In the SEUS, we calculated the linear regression between OA and sulfate in

Figure 3a following the method of Malm et al. (2017). Each data point represents the SPEI bin-averaged value of

OA and sulfate from each grid cell. The bins are divided to have approximately the same number of samples

following Xie et al (2019). Only the grids with all five SPEI bins present are used (N=673), which include more than

95% of the total grids (687). Thus, the binned regression calculation can represent the regional conditions of each

SPEI bin. The resulting linear lines and formula are also displayed in Figure 3a. Here the slope calculation is

different from Zheng et al. (2020), in which they averaged OA and sulfate across all the sites in the SEUS and

performed the linear regression temporally. We adopted a spatial calculation of the linear slopes for two reasons: (1)

Averaging across all the sites/grids will significantly reduce the number of data points after the allocation among

SPEI bins; (2) The regional mean of SPEI may average out some drought signals because drought is grid specific

and can differ spatially within the SEUS (Ford et al., 2014). Despite the different methods used, the linear slope in

our calculation (0.56) under non-drought conditions is similar to that of Zheng et al. (2020) using SEARCH

(SouthEastern Aerosol Research and Characterization) sites (0.51). Therefore, our linear slope calculation method

reproduces the sensitivity of OA to sulfate reported by the existing studies.

As SPEI changes from positive (non-drought) to negative (drought), the slope between OA and sulfate becomes

increasingly higher, ranging from 0.56 to 0.79. This indicates more OA formations per unit increase in sulfate as

drought severity intensifies~~deteriorates~~. Although high correlations do not necessarily indicate causal relationships,

218 the chemical mechanism of IEPOX SOA formation with the presence of sulfate is well documented (e.g.,

219 Shrivastava et al., 2017). The higher sensitivities of OA to sulfate under droughts can be explained by the

220 increasingly higher isoprene concentrations as shown in our previous studies in the SEUS (Li et al., 2022; Wang et

221 al., 2022b), resulting in more IEPOX in the atmosphere to be further converted to particle phase catalyzed by

222 sulfate. In addition, the formation of monoterpene-derived organosulfates, a major component of IEPOX SOA, is

223 also dependent on sulfate (D'Ambro et al., 2019) and the biogenic emissions of monoterpenes are likely to be

224 intensified during droughts (Llusià et al., 2008; Wu et al., 2015). Organosulfates originated from anthropogenic

225 precursors are also reported by some studies (Riva et al., 2015; Le Breton et al., 2018), but they are mainly found in

226 highly polluted urban areas. We further reproduced Figure 3a using detrended OA and sulfate data, which can

227 remove the effects of anthropogenic emissions (Figure S3b). A similar pattern of the gradually increasing slope from

228 the wettest (slope=0.18) to the driest (slope=0.48) SPEI bin was found, which verifies the stronger dependence of

229 OA on sulfate under droughts is mainly caused by biogenic sources.

230

231
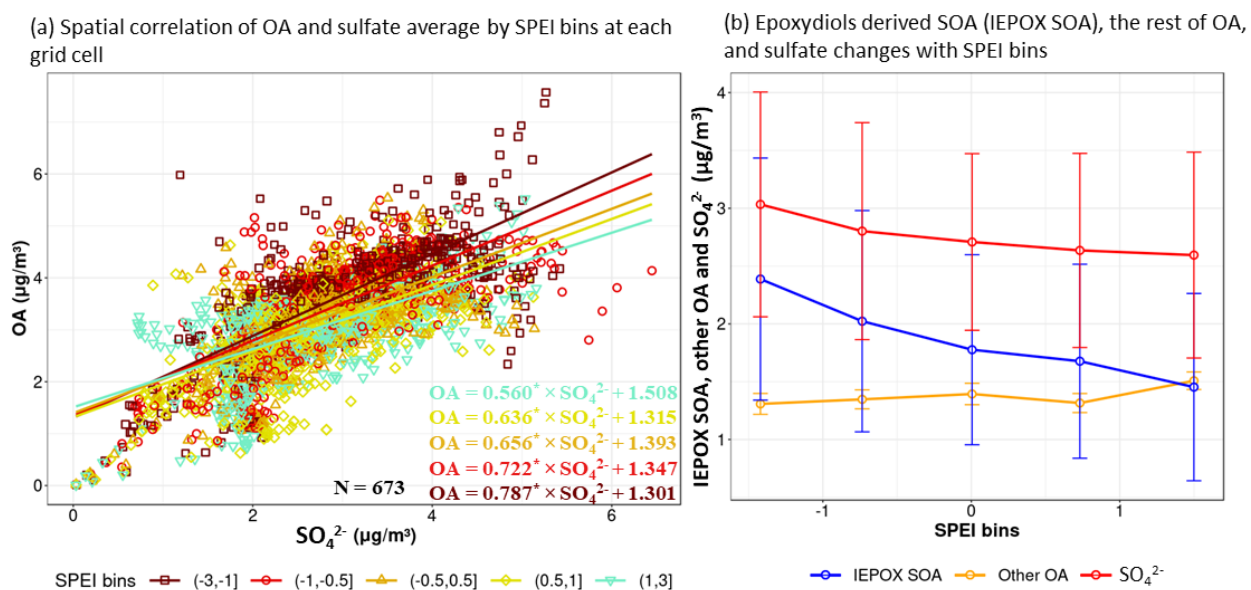
Figure 3. (a) Scatter plot of the SPEI bin-averaged sulfate and OA at each grid in the SEUS with solid lines representing
the linear regressions of OA and sulfate. The corresponding linear formula of each SPEI bin is listed in the bottom-right
corner with N indicating the number of data points for each regression calculation. The star marks in the formula indicate
the regression significance at a 95% confidence level. (b) The epoxydiols derived SOA (IEPOX SOA), other SOA, and
sulfate changes with SPEI derived from the linear regressions in a. Vertical bars indicate one standard deviation.

237 The intercept of the linear regression can be interpreted as other OA components that are not associated with sulfate-

238 catalyzed IEPOX SOA, such as POA and anthropogenic SOA (Malm et al., 2017). Figure 3b shows that the

239 intercepts (other OA) are stable among the five SPEI bins with a less than $0.2\ \mu g\,m^{-3}$ (15%) difference. The

240 differences of regional mean OA minus the intercepts can then be considered as IEPOX SOA related to sulfate. The

241 resulting estimate of IEPOX SOA is $1.45\ \mu g\,m^{-3}$, $1.68\ \mu g\,m^{-3}$, $1.78\ \mu g\,m^{-3}$, $2.02\ \mu g\,m^{-3}$ and $2.39\ \mu g\,m^{-3}$ for the five

242 SPEI bins ranging from wet to dry conditions. These values correspond to an increase of $0.30\ \mu g\,m^{-3}$ IEPOX SOA

243 per unit decrease in SPEI. Interestingly, there is also an increasingly higher sulfate level from wet to dry SPEI bins

244 with a mean value of 2.59 µg m^{-3}, 2.63 µg m^{-3}, 2.71 µg m^{-3}, 2.80 µg m^{-3} and 3.03 µg m^{-3}, respectively,

245 corresponding to an overall increase rate of 0.14 µg m^{-3} sulfate per unit decrease of SPEI. Therefore, the increase of

246 OA in the SEUS under droughts is largely caused by the boosted formation of BSOA due to the concurrent increase

247 in VOC emissions and sulfate. This is consistent with the modeling case study by Zhao et al. (2019) who found that

248 98% of the SOA increase during drought in the SEUS is of biogenic origin. It is noted that the approximation of

249 IEPOX SOA here is the upper limit of BSOA since other processes that can lead to the simultaneous changes of

250 sulfate and OA, such as wildfire, are miscounted as BSOA in the calculation. Further analysis is needed to attribute

251 the changes of SOA to different sources more accurately.
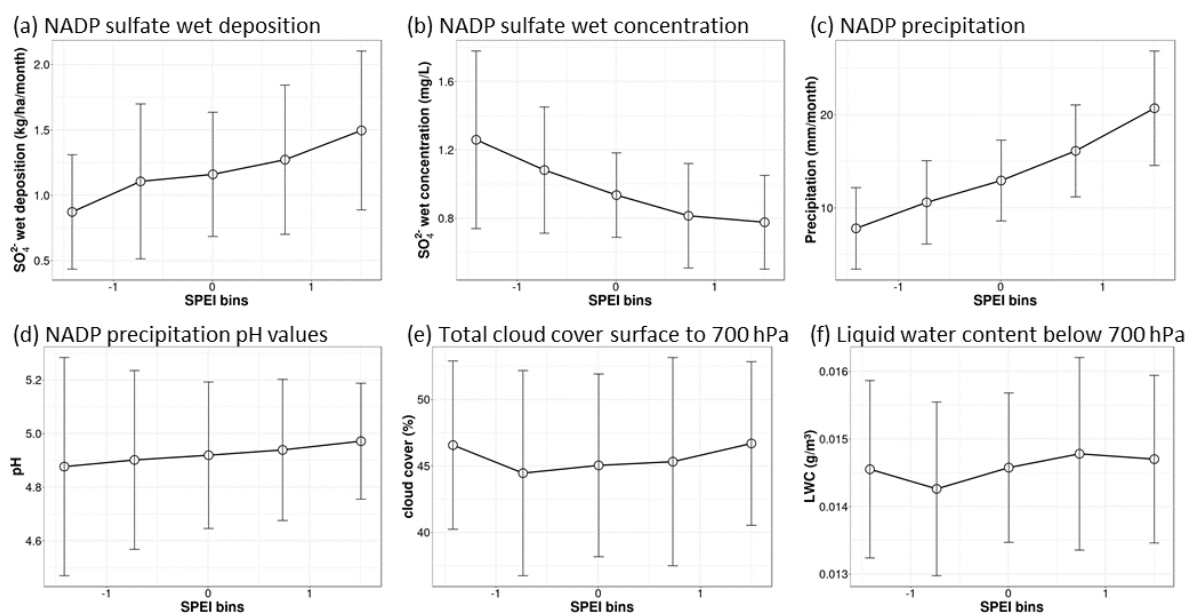
252
253 **Figure 4. SPEI bin-averaged sulfate wet deposition (a), wet concentration (b), precipitation amount (c), precipitation pH**
254 **values (d) from the NADP network, and the total cloud cover (e) and liquid water content (LWC; f) below 700 hPa from**
255 **the MODIS satellite in the SEUS. Vertical bars indicate one standard deviation.**

256
257 The source and sink of atmospheric sulfate are greatly affected by clouds and precipitation because most of the

258 sulfate is formed in clouds and efficiently removed by wet scavenging (Barth et al., 2000; Rasch et al., 2000; Berg et

259 al., 2015). Thus, it is understandable that sulfate is sensitive to drought considering both clouds and precipitation are

260 significantly modulated under droughts. To further investigate the processes causing the increase of sulfate, we

261 analyzed sulfate wet deposition, wet concentration, precipitation amount, and pH values (Figure 4a-d) from the

262 NADP network. There is a decreasing trend of sulfate wet deposition from 1.50 kg ha^{-1} month^{-1} at the wettest (SPEI

263 > 1) to 0.87 kg ha^{-1} month^{-1} at the driest (SPEI < -1) level. The corresponding reduction in precipitation is 62%.

264 Since sulfate wet deposition is calculated using sulfate wet concentration weighted by precipitation, the 50%

265 decrease of sulfate wet deposition is driven by the reduced precipitation, which outweighs the increase of sulfate

266 concentrations.

267 The low level (below 700 hPa) cloud cover and liquid water content (LWC) are not highly sensitive to droughts with
268 less than 2% and 4% changes among the five SPEI bins, respectively (Figure 4e-f). Thus, the increase of sulfate wet
269 concentrations in precipitation is likely indicative of an enhanced formation of aqueous sulfate in the clouds, which
270 then precipitates. Alternatively, gas phase production of sulfate can also be elevated under droughts due to more
271 sulfur dioxide (SO_2) emissions (e.g. from increased electricity generation and fires) and higher temperatures (Tai et
272 al., 2010; Wang et al., 2017), and then washed out by rainwater droplets causing higher sulfate wet concentrations in
273 precipitation. Either of these two pathways suggests that there is higher sulfate formation under droughts which
274 contributes to the enhanced sulfate besides reduced wet deposition. Furthermore, the mean pH value drops steadily
275 with dryness levels from 4.98 to 4.87, which further intensifies the acid-catalyzed IEPOX ring opening and leads to
276 faster BSOA formation (Surratt et al., 2010). Although the rate of IEPOX SOA formation is slower in cloud water
277 compared to aerosol particles due to its relatively higher pH values (Gaston et al., 2014), the large liquid water
278 content of clouds, which promotes dissolution, could lead to significant IEPOX SOA formation. Based on a box
279 model simulation conducted by Tsui et al (2019), increasing pH values in cloud water while keeping the other
280 factors constant results in a slower rate of IEPOX SOA formation. Additionally, cloud water processing at pH ≤ 4
281 can produce more IEPOX SOA than aerosol particles. Despite the average pH value of ~5 across the SEUS region,
282 some sites may experience more acidic rainwater in drought months. During the study period, we found two sites in
283 Georgia and North Carolina with pH less than 4 and their corresponding SPEI values are –0.98 and –1.39.
284 Therefore, droughts are likely to reduce cloud pH values lower enough at some locations and favorable for
285 significant IEPOX SOA formation.

286 Using the same approach as in the SEUS, we calculated the SPEI bin-averaged OA and OA wildfire emissions from
287 the GFED4 inventory in the PNW region shown in Figure 5. OA fire emissions grow from 0.09×10^7 g per month at
288 the wettest level to 4.94×10^7 g per month at the second driest level (SPEI between -1.5 and -1), followed by a small
289 drop to 4.17×10^7 g per month at the driest level (SPEI less than -1.5). This drop is likely caused by the reduction in
290 the supply of fire fuel load under extreme drought conditions (Scasta et al., 2016). Overall, OA fire emissions
291 increase by 1.44×10^7 g per unit decrease of SPEI per month. The mass concentrations of OA resemble the changes
292 of OA fire emissions with an overall increase rate of 1.01 µg m^{-3} per unit decrease of SPEI, which indicates more
293 wildfire emissions are the major driver of the higher OA concentrations in the PNW.
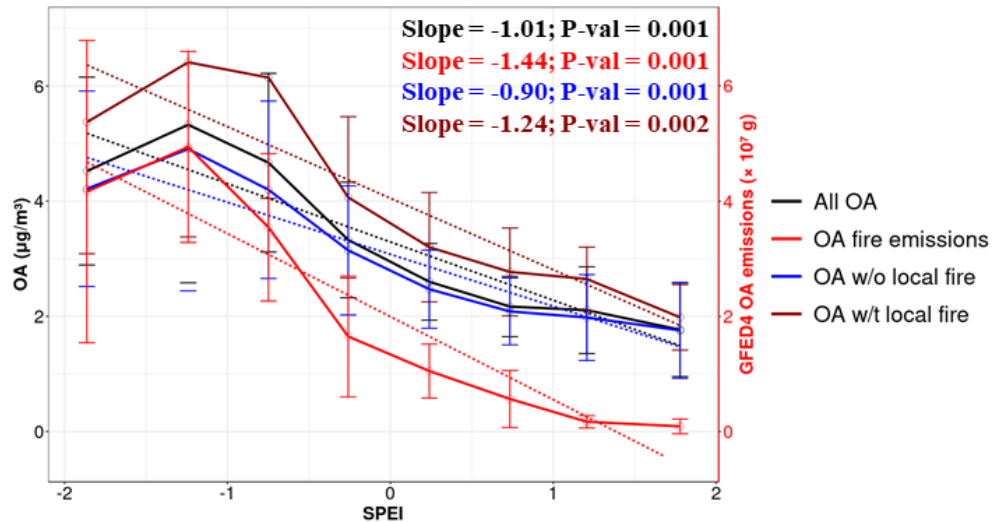
Figure 5. Mean (point) and one standard deviation (vertical bar) of OA (black line), wildfire OA emissions from GFED4 inventory (bright red line; right axis), and OA with (dark red line) and without (blue line) local fire occurrence within each SPEI bin. The dashed lines represent the linear regression with the slopes (Slope) and P-values (P-val) of each variable listed in the top-right corner.

To better quantify the contributions of wildfire, we further separated OA values into those with local fire influences if OA fire emissions are greater than zero at each grid in each month and those without local fire influences if zero fire emissions are found. The time series of OA grouped by periods with and without wildfire emissions within each SPEI bin (Figure S4) shows that the two groups have nearly identical temporal coverage with data found in almost all years within most SPEI bins, which indicates the separation does not cause temporal inconsistency. We admit that this separation relies on the accuracy of fire emissions and cannot rule out the effects of the long-range transported OA from other regions, especially for the widespread drought events. As a result, it may overestimate OA values with no local fire occurrence. With this caveat in mind, we calculated the local fire effects as the difference between OA with and without fire emissions within each drought bin. Under the wettest conditions, there is a minor difference of 0.23 $\mu g \, m^{-3}$ between OA with and without local fire effects, while this number becomes four to eight times higher under droughts (SPEI < zero). The local fire-affected OA with one unit decrease of SPEI also increases by 0.34 $\mu g \, m^{-3}$ faster than that without local fire occurrence. This illustrates the considerable contributions of local wildfire emissions to the changes of OA under droughts. Other processes, such as long-range transported aged OA and locally produced BSOA, may also contribute to the differences if their contributions correlate with local fire emissions.

In summary, there is an increasing sensitivity of OA to sulfate as drought conditions worsen in the SEUS, driven by the heightened biogenic VOC emissions and the subsequent formation of IEPOX SOA. Sulfate levels also rise under droughts, influenced mainly by the reduced precipitation and the potentially increased aqueous and gas-phase sulfate production. In the PNW, OA and OA wildfire emissions exhibit a close correlation, indicating that wildfire emissions significantly drive higher OA concentrations therein.

3.3 CMIP6 Models Simulated Organic Aerosol Response to Drought

In this section, we evaluated the surface OA concentrations from ten CMPI6 models regarding their capability in predicting the observed SPEI-OA relationships over the CONUS during JJA 1998-2014. OA values from each model were interpolated linearly to match the spatial resolution of the gridded observational dataset. Figure 6a-j show the spatial distributions of the slopes between SPEI and OA simulated by each model. Compared with the observed slopes in Figure 2a, all models capture the strong negative slopes of more than 2 $\mu g\,m^{-3}$ per unit decrease of SPEI in the PNW region except for GFDL-ESM4 which shows a much smaller slope of less than 1 $\mu g\,m^{-3}$ per SPEI. This indicates the CMIP6 models correctly represent the sign and magnitude of the changes in OA fire emissions with droughts. By contrast, all the models have difficulties in reproducing the observed linear relationships between OA and SPEI in the SEUS. Compared to the significantly negative slope from observations, most of the models display insignificant or even positive slopes in the SEUS. BCC-ESM1, MRI-ESM2-0, and Nor-ESM2-LM show negative slopes only in part of the SEUS grids.

We also evaluated model predicted average OA enhancement under server droughts relative to non-drought periods in PNW and SEUS (Figure 6k). In the PNW region, CESM2-WACCM simulates an increase of OA mass concentration by 2.20 $\mu g\,m^{-3}$, closest to the observed value of 2.41 $\mu g\,m^{-3}$, followed by UKESM1-0-LL and CNRM-ESM2-1 with an enhancement of 1.74 $\mu g\,m^{-3}$ and 1.64 $\mu g\,m^{-3}$, respectively. GFDL-ESM4 shows the highest underestimation of the OA enhancement by 2 $\mu g\,m^{-3}$ (83%), consistent with its smallest slopes shown in Figure 6e. Smaller underestimations are found in other models, ranging from 0.96 $\mu g\,m^{-3}$ (40%) for MRI-ESM2-0 to 1.4 $\mu g\,m^{-3}$ (58%) for EC-Earth3-AerChem. In the SEUS, all the ten models underpredict the observed OA increase of 0.57 $\mu g\,m^{-3}$ with the two lowest underestimations of 0.21 $\mu g\,m^{-3}$ (37%) and 0.27 $\mu g\,m^{-3}$ (47%) found for Nor-ESM2-LM and MIRCO6, respectively. The other eight models show marginal OA enhancements between 0.02 $\mu g\,m^{-3}$ to 0.21 $\mu g\,m^{-3}$ or even a decrease (GISS-E2-1-G), indicating the incapabilities of these models in predicting OA changes in the SEUS under droughts.
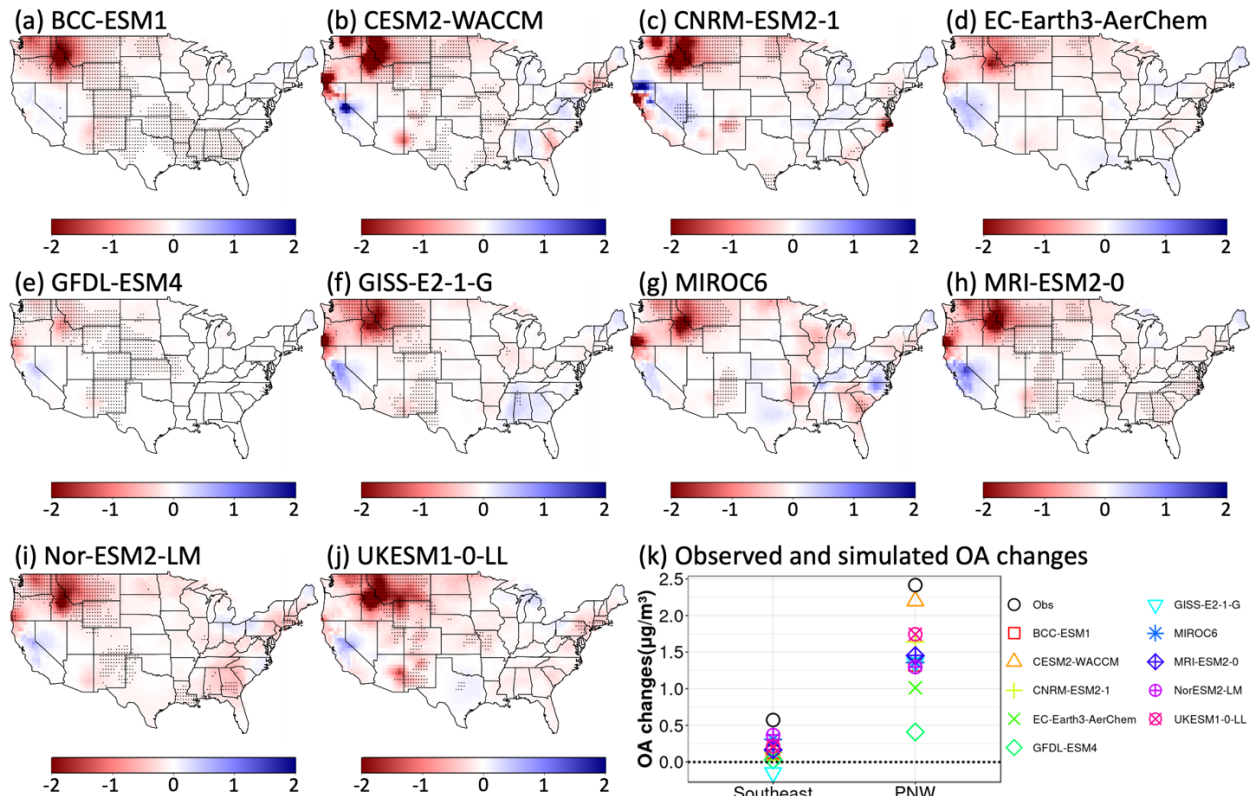
343
344 **Figure 6. (a-j) Slopes between CMIP6 model simulated OA and SPEI from 1998 to 2014 during summertime with black**
345 **dots indicating the P-values less than 0.05. (k) Observed and simulated OA changes under severe droughts relative to non-**
346 **drought conditions during the same study period in the PNW and SEUS regions.**

347
348 The poor model performance in capturing the OA changes under severe drought in the SEUS inspires us to conduct
349 a further regional analysis following Section 3.2. The observed and simulated changes of SEUS-mean OA, sulfate,
350 and their slopes within each SPEI bin are shown in Figure 7a-c, respectively. The modeled slopes are calculated in
351 the same way as observations (Figure 3a) and the associated scatter plot is shown in Figure S5. For the absolute OA
352 mass concentrations, UKESM1-0-LL has the best predictions with a less than 0.5 $\mu g\,m^{-3}$ mean bias in each SPEI
353 bin. CESM2-WACCM, CNRM-ESM2-1, EC-Earth3-AerChem, MICRO6, and NorESM2-LM overestimate OA
354 values, while the other four models show an underestimation. For the sensitivity of OA to droughts, NorESM2-LM
355 performs the best with an increase rate of 0.13 $\mu g\,m^{-3}$ per unit decrease of SPEI, although the rate is only 50% of the
356 observed value of 0.25 $\mu g\,m^{-3}$. This is consistent with the result that this model has the lowest underestimation of
357 OA enhancement under severe droughts. Higher underestimations of the OA sensitivity to droughts are found in
358 MRI-ESM2-0, BCC-ESM1, and GFDL-ESM4 with a respective change rate of 0.09 $\mu g\,m^{-3}$, 0.06 $\mu g\,m^{-3}$ and 0.02
359 $\mu g\,m^{-3}$ per SPEI. On the contrary, GISS-E2-1-G simulates a decrease in OA by 0.04 $\mu g\,m^{-3}$ per unit decrease of
360 SPEI, which is consistent with the negative OA changes under severe droughts. The rest of the models do not have a
361 statistically significant change rate of OA with droughts at a 95% confidence level.

(a) Observed and simulated OA changes with SPEI in the SEUS

(b) Observed and simulated sulfate changes with SPEI in the SEUS

(c) Observed and simulated slopes between OA and sulfate changes with SPEI in the SEUS
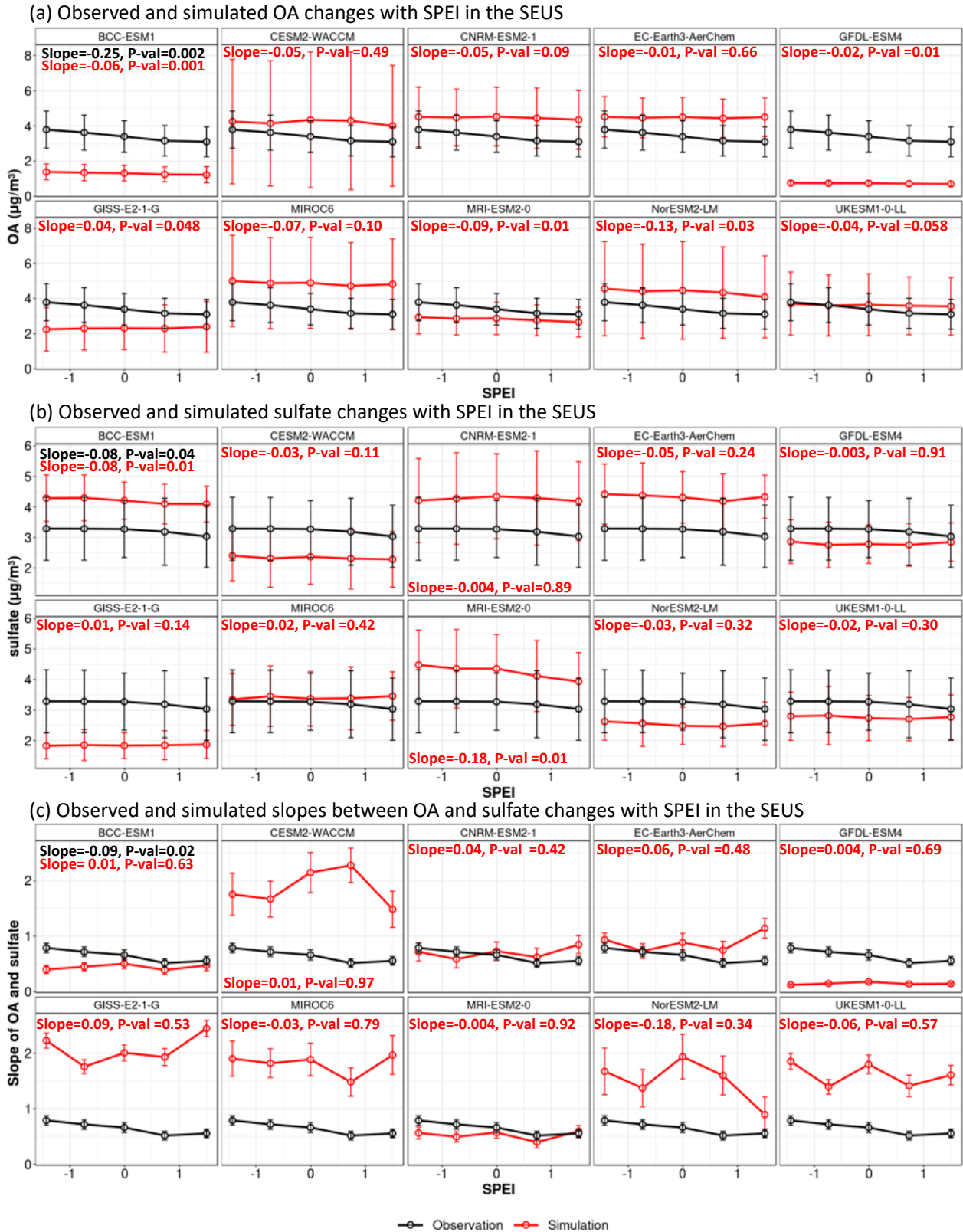
362
363 **Figure 7. SPEI bin-averaged values of OA (a), sulfate (b), and slopes of OA and sulfate (c) from observations (black lines)**
364 **and simulations (red lines) in the SEUS. Vertical bars indicate one standard deviation. The numbers in each subplot indicate**
365 **the slopes (Slope) and P-values (P-val) of the linear regression between each variable and SPEI.**

366
367 As described in Figure 3, the increase of OA under droughts in the SEUS is due to the concurrent increase of sulfate

368 and biogenic VOC emissions. To investigate if the models have this mechanism, we also evaluated the modeled

369 sensitivities of sulfate and the OA-sulfate slopes to SPEI. Only two models, BCC-ESM1 and MRI-ESM2-0, have

370 statistically significant increase rates of sulfate with the decrease of SPEI, despite their overestimation of ~1 $\mu g\,m^{-3}$

371 (30%) in terms of the absolute sulfate concentrations. BCC-ESM1 predicts the same change rate as observations

372 with a value of 0.08 $\mu g\,m^{-3}$ per unit change of SPEI, while MRI-ESM2-0 predicts a rate of 0.18 $\mu g\,m^{-3}$, more than

373 doubled the observed rate. ~~The slopes between OA and sulfate derived from these two models are also the closest to~~

374 ~~the observed value of 0.53 in the two wettest SPEI bins, indicating the dependence of IEPOX SOA formation on~~

375 ~~sulfate is well captured by these two models when no drought occurs.~~ For the slopes between OA and sulfate,

376 ~~h~~However, all models~~the slopes stay stable among SPEI bins and~~ cannot reproduce the observed increase rate of

377 0.09 per unit decrease of SPEI. ~~Similarly, this feature is not captured by the other eight models, although some of~~

378 ~~them show big variabilities (e.g., CESM2-WACCM and NorESM2-LM).~~ This suggests either an insensitivity ~~or a~~

379 ~~non-persistent change~~ of biogenic VOC emissions~~isoprene~~ in response to drought~~s severity~~ or a lack of explicit

380 aqueous chemistry for SOA formation in the~~all~~ models. ~~In addition, seven out of ten models, excluding BCC-ESM1,~~

381 ~~MRI-ESM2-0, and GFDL-ESM4, generally overestimate the slopes between OA and sulfate regardless of the~~

382 ~~dryness conditions, signifying an overdependence of the formation of IEPOX SOA on sulfate in these models.~~ For a

383 further investigation, we summarized how SOA is treated in each model (Table S1). In fact, SOA schemes in the 10

384 CMIP6 models are simplified to reduce computational cost as the climate models need to perform hundreds of years

385 of simulations with many ensemble members (Eyring et al., 2016). BCC-ESM1 and CESM2-WACCM use a

386 volatility basis set (VBS) approach that categorizes VOCs based on their volatility and simulates the chemical aging

387 process that leads to the formation of SOA. In CNRM-ESM2-1, SOA is prescribed from a monthly inventory

388 without inline calculation. EC-Earth3-AerChem, GISS-E2-1-G, and MIROC6 include the two-product scheme, in

389 which VOC oxidation leads to non-volatile and semi-volatile products. The rest of the models assume a fixed

390 percentage of yield from the emissions of VOCs. In short, the heterogeneous formation of IEPOX SOA through

391 reactive uptake on aqueous sulfate is not parameterized in the models. Therefore, the linear relationship between OA

392 and sulfate in the models is not indicative of the mechanistic dependence of OA on sulfate as demonstrated in

393 observations. Similar anthropogenic sources (e.g., fossil fuel combustion) and photochemical oxidants (e.g., O3 and

394 OH) leading to the simultaneous production of sulfate and OA can also result in positive correlations (Zhang et al.,

395 2011). The lack of the IEPOX SOA formation mechanism further explains why the enhancements of OA in the

396 SEUS are barely captured by these models.

397 To sum up, most of the models can represent the linear relationships between OA and SPEI in the PNW region with

398 CESM2-WACCM and GFDL-ESM4 performing the best and worst in predicting the OA enhancement under severe

399 droughts. However, all the models face challenges in capturing the OA increases under droughts in the SEUS, with

400 Nor-ESM2-LM and MIRCO6 showing relatively better performance indicated by their lower underestimation of OA

401 enhancement. These challenges are mainly caused by the lack of parameterizations of the aqueous formation of

402 IEPOX SOA and the model deficiencies in capturing the increase pattern of sulfate as drought intensifies.

4 Conclusions

In this study, the changes in organic aerosol (OA) in response to drought in the CONUS were examined. We first displayed the spatial patterns of OA under non-drought and severe drought conditions and found most of the CONUS experiences an abnormally higher level of OA by an average of 0.72 $\mu g\,m^{-3}$ relative to wet and normal conditions. Regionally, the highest average increase occurs in the PNW and SEUS areas by 1.79 $\mu g\,m^{-3}$ (112 %) and 0.92 $\mu g\,m^{-3}$ (33 %), respectively. The concurrent enhancement of wildfire OA emissions in the PNW and sulfate in the SEUS provides more insights into an in-depth investigation over these two regions.

In the SEUS, a linear regression between OA and sulfate was applied to estimate the amount of IEPOX SOA and other OA. Results from this simplified method indicate that the IEPOX SOA drives the increase of total OA from wet to dry conditions while other OA stays stable. Both the increase of biogenic VOC emissions and sulfate under droughts lead to the enhancement of IEPOX SOA. Data from the NADP network shows that up to 62% lower precipitation under droughts induces slower sulfate wet deposition rates and thus leaves more sulfate in the atmosphere. Higher sulfate wet concentration in the precipitation indicates more in-cloud and/or gas-phase sulfate production under droughts since cloud cover and liquid content do not show a strong sensitivity to droughts.

In the PNW, there is an overall increase of 1.44×10^7 g in the monthly OA wildfire emissions per unit decrease of SPEI, which is the main driver of the elevated OA. There is a plateau of the OA fire emissions with SPEI between -1.5 and -1, followed by a drop with SPEI less than -1.5. This implies that wildfire activities are not linearly related to moisture and are also limited by the availability of fuel load. Dividing OA into groups with or without local fire influence, we found that local fire events can increase the OA concentrations by four to eight times relative to those without fire activities. Future work is needed to further investigate the changes in OA from other sources, such as long-range transported OA and BSOA, in this region.

The evaluation of surface OA concentrations from ten CMIP6 models provides valuable insights into their predictive capabilities in capturing the observed relationships between SPEI and OA over the CONUS. All the models are found to successfully capture the negative slopes in the PNW area, indicating correct sensitivities of OA wildfire emissions to droughts in these models. However, deficiencies are revealed in the SEUS with most models displaying insignificant or positive slopes between OA and SPEI as opposed to significantly negative slopes from observations. The assessment of average OA enhancement during severe droughts relative to non-drought periods further underscores the models' varying degrees of accuracy in simulating OA response to drought. In the PNW, CESM2-WACCM stands out with its simulated OA increase of 2.20 $\mu g\,m^{-3}$ being closest to the observed value of 2.41 $\mu g\,m^{-3}$, while GFDL-ESM4 exhibits the highest underestimation of OA enhancement by 2 $\mu g\,m^{-3}$ (83%). In the SEUS, all models consistently underpredict the observed OA increases, highlighting their limitations in predicting OA changes in this region under drought conditions. These limitations can be mainly attributed to the insensitivities of sulfate to SPEI and the model deficiencies in the parameterization of the IEPOX SOA dependence on inorganic sulfate.

437   This study reveals the key drivers of the enhanced OA mass concentrations in the CONUS, including higher wildfire
438   emissions and the simultaneous increase in biogenic VOC emissions and inorganic sulfate, which highlights the
439   complex physical and chemical processes involved in the aerosol composition changes under droughts. The
440   discrepancies in simulating OA enhancements during severe droughts underscore the need for ongoing model
441   improvement, particularly in accurately representing the emissions of biogenic isoprene and monoterpene, the life
442   cycle of sulfate, and their intricate interactions. Addressing these limitations will be crucial for enhancing the
443   reliability of climate models and their ability to predict the impact of future droughts on atmospheric composition
444   and air quality in the CONUS.

Data availability

446   Monthly SPEI data is obtained from https://spei.csic.es/spei_database_2_6 (Vicente-Serrano et al., 2010).
447   Observations from the IMPROVE and NADP network are downloaded from
448   https://views.cira.colostate.edu/fed/QueryWizard/ (FED, 2023). GFED4 wildfire emission inventory and MODIS
449   satellite cloud cover data are archived at https://www.geo.vu.nl/~gwerf/GFED/GFED4/ (Giglio et al., 2013) and
450   https://asdc.larc.nasa.gov/project/CERES/CER_SSF1deg-Month_Terra-MODIS_Edition4A (NASA, 2015),
451   respectively. The CMIP6 model outputs are publicly available online from the Earth System Federation Grid nodes.

Competing interests

453   The authors declare that they have no conflict of interest.

Author contributions

455   YW conceived the research idea. WL conducted the analysis. Both authors contributed to the preparation of the
456   manuscript.

Acknowledgments

458   The authors acknowledge researchers from the IMPROVE and NADP networks for making surface aerosol mass
459   and deposition observations. We thank individuals and groups from the Climatology and Climate Services
460   Laboratory for creating the SPEI dataset. The authors also thank the modeling groups participating in the CMIP6
461   AerChemMIP project for making the surface aerosol species outputs available.

Financial support

463   This research has been supported by the National Oceanic and Atmospheric Administration through the
464   Atmospheric Chemistry, Carbon Cycle and Climate (AC4) Program (grant no. NA19OAR4310177).

References

Barth, M. C., Rasch, P. J., Kiehl, J. T., Benkovitz, C. M., and Schwartz, S. E.: Sulfur chemistry in the National Center for Atmospheric Research Community Climate Model: Description, evaluation, features, and sensitivity to aqueous chemistry, J. Geophys. Res. Atmospheres, 105, 1387–1415, https://doi.org/10.1029/1999JD900773, 2000.

Berg, L. K., Shrivastava, M., Easter, R. C., Fast, J. D., Chapman, E. G., Liu, Y., and Ferrare, R. A.: A new WRF-Chem treatment for studying regional-scale impacts of cloud processes on aerosol and trace gases in parameterized cumuli, Geosci. Model Dev., 8, 409–429, https://doi.org/10.5194/gmd-8-409-2015, 2015.

Borlina, C. S. and Rennó, N. O.: The impact of a severe drought on dust lifting in California's Owens Lake area, Sci. Rep., 7, 1784, https://doi.org/10.1038/s41598-017-01829-7, 2017.

Brégonzio-Rozier, L., Giorio, C., Siekmann, F., Pangui, E., Morales, S. B., Temime-Roussel, B., Gratien, A., Michoud, V., Cazaunau, M., DeWitt, H. L., Tapparo, A., Monod, A., and Doussin, J.-F.: Secondary organic aerosol formation from isoprene photooxidation during cloud condensation–evaporation cycles, Atmospheric Chem. Phys., 16, 1747–1760, https://doi.org/10.5194/acp-16-1747-2016, 2016.

Brilli, F., Barta, C., Fortunati, A., Lerdau, M., Loreto, F., and Centritto, M.: Response of isoprene emission and carbon metabolism to drought in white poplar (Populus alba) saplings, New Phytol., 175, 244–254, https://doi.org/10.1111/j.1469-8137.2007.02094.x, 2007.

Carslaw, K. S., Lee, L. A., Reddington, C. L., Pringle, K. J., Rap, A., Forster, P. M., Mann, G. W., Spracklen, D. V., Woodhouse, M. T., Regayre, L. A., and Pierce, J. R.: Large contribution of natural aerosols to uncertainty in indirect forcing, Nature, 503, 67–71, https://doi.org/10.1038/nature12674, 2013.

Cook, B. I., Mankin, J. S., and Anchukaitis, K. J.: Climate change and drought: From past to future, Curr. Clim. Change Rep., 4, 164–179, https://doi.org/10.1007/s40641-018-0093-2, 2018.

D'Ambro, E. L., Schobesberger, S., Gaston, C. J., Lopez-Hilfiker, F. D., Lee, B. H., Liu, J., Zelenyuk, A., Bell, D., Cappa, C. D., Helgestad, T., Li, Z., Guenther, A., Wang, J., Wise, M., Caylor, R., Surratt, J. D., Riedel, T., Hyttinen, N., Salo, V.-T., Hasan, G., Kurtén, T., Shilling, J. E., and Thornton, J. A.: Chamber-based insights into the factors controlling epoxydiol (IEPOX) secondary organic aerosol (SOA) yield, composition, and volatility, Atmospheric Chem. Phys., 19, 11253–11265, https://doi.org/10.5194/acp-19-11253-2019, 2019.

Danabasoglu, G., Lamarque, J.-F., Bacmeister, J., Bailey, D. A., DuVivier, A. K., Edwards, J., Emmons, L. K., Fasullo, J., Garcia, R., Gettelman, A., Hannay, C., Holland, M. M., Large, W. G., Lauritzen, P. H., Lawrence, D. M., Lenaerts, J. T. M., Lindsay, K., Lipscomb, W. H., Mills, M. J., Neale, R., Oleson, K. W., Otto-Bliesner, B., Phillips, A. S., Sacks, W., Tilmes, S., van Kampenhout, L., Vertenstein, M., Bertini, A., Dennis, J., Deser, C., Fischer, C., Fox-Kemper, B., Kay, J. E., Kinnison, D., Kushner, P. J., Larson, V. E., Long, M. C., Mickelson, S., Moore, J. K., Nienhouse, E., Polvani, L., Rasch, P. J., and Strand, W. G.: The Community Earth System Model Version 2 (CESM2), J. Adv. Model. Earth Syst., 12, e2019MS001916, https://doi.org/10.1029/2019MS001916, 2020.

Dawson, J. P., Adams, P. J., and Pandis, S. N.: Sensitivity of $PM_{2.5}$ to climate in the Eastern US: a modeling case study, Atmospheric Chem. Phys., 7, 4295–4309, https://doi.org/10.5194/acp-7-4295-2007, 2007.

Dennison, P. E., Brewer, S. C., Arnold, J. D., and Moritz, M. A.: Large wildfire trends in the western United States, 1984–2011, Geophys. Res. Lett., 41, 2928–2933, https://doi.org/10.1002/2014GL059576, 2014.

Dunne, J. P., Horowitz, L. W., Adcroft, A. J., Ginoux, P., Held, I. M., John, J. G., Krasting, J. P., Malyshev, S., Naik, V., Paulot, F., Shevliakova, E., Stock, C. A., Zadeh, N., Balaji, V., Blanton, C., Dunne, K. A., Dupuis, C., Durachta, J., Dussin, R., Gauthier, P. P. G., Griffies, S. M., Guo, H., Hallberg, R. W., Harrison, M., He, J., Hurlin, W., McHugh, C., Menzel, R., Milly, P. C. D., Nikonov, S., Paynter, D. J., Ploshay, J., Radhakrishnan, A., Rand, K., Reichl, B. G., Robinson, T., Schwarzkopf, D. M., Sentman, L. T., Underwood, S., Vahlenkamp, H., Winton, M., Wittenberg, A. T., Wyman, B., Zeng, Y., and Zhao, M.: The GFDL Earth System Model Version 4.1 (GFDL-ESM

4.1): Overall Coupled Model Description and Simulation Characteristics, J. Adv. Model. Earth Syst., 12, e2019MS002015, https://doi.org/10.1029/2019MS002015, 2020.

Eyring, V., Bony, S., Meehl, G. A., Senior, C. A., Stevens, B., Stouffer, R. J., and Taylor, K. E.: Overview of the Coupled Model Intercomparison Project Phase 6 (CMIP6) experimental design and organization, Geosci. Model Dev., 9, 1937–1958, https://doi.org/10.5194/gmd-9-1937-2016, 2016.

Fang, Y., Fiore, A. M., Horowitz, L. W., Gnanadesikan, A., Held, I., Chen, G., Vecchi, G., and Levy, H.: The impacts of changing transport and precipitation on pollutant distributions in a future climate, J. Geophys. Res. Atmospheres, 116, https://doi.org/10.1029/2011JD015642, 2011.

FED: The Federal Land Manager Environmental Database query wizard, FED, https://views.cira.colostate.edu/fed/QueryWizard/ (last access: 27 December 2023), 2023.

Gaston, C. J., Riedel, T. P., Zhang, Z., Gold, A., Surratt, J. D., and Thornton, J. A.: Reactive Uptake of an Isoprene-Derived Epoxydiol to Submicron Aerosol Particles, Environ. Sci. Technol., 48, 11178–11186, https://doi.org/10.1021/es5034266, 2014.

Giglio, L., Randerson, J. T., and van der Werf, G. R.: Analysis of daily, monthly, and annual burned area using the fourth-generation global fire emissions database (GFED4), J. Geophys. Res. Biogeosciences, 118, 317–328, https://doi.org/10.1002/jgrg.20042, 2013.

Gilman, J. B., Lerner, B. M., Kuster, W. C., Goldan, P. D., Warneke, C., Veres, P. R., Roberts, J. M., de Gouw, J. A., Burling, I. R., and Yokelson, R. J.: Biomass burning emissions and potential air quality impacts of volatile organic compounds and other trace gases from fuels common in the US, Atmospheric Chem. Phys., 15, 13915–13938, https://doi.org/10.5194/acp-15-13915-2015, 2015.

Gomez, J., Allen, R. J., Turnock, S. T., Horowitz, L. W., Tsigaridis, K., Bauer, S. E., Olivié, D., Thomson, E. S., and Ginoux, P.: The projected future degradation in air quality is caused by more abundant natural aerosols in a warmer world, Commun. Earth Environ., 4, 1–11, https://doi.org/10.1038/s43247-023-00688-7, 2023.

Gorham, K. A., Raffuse, S. M., Hyslop, N. P., and White, W. H.: Comparison of recent speciated PM2.5 data from collocated CSN and IMPROVE measurements, Atmos. Environ., 244, 117977, https://doi.org/10.1016/j.atmosenv.2020.117977, 2021.

Hallquist, M., Wenger, J. C., Baltensperger, U., Rudich, Y., Simpson, D., Claeys, M., Dommen, J., Donahue, N. M., George, C., Goldstein, A. H., Hamilton, J. F., Herrmann, H., Hoffmann, T., Iinuma, Y., Jang, M., Jenkin, M. E., Jimenez, J. L., Kiendler-Scharr, A., Maenhaut, W., McFiggans, G., Mentel, T. F., Monod, A., Prévôt, A. S. H., Seinfeld, J. H., Surratt, J. D., Szmigielski, R., and Wildt, J.: The formation, properties and impact of secondary organic aerosol: current and emerging issues, Atmospheric Chem. Phys., 9, 5155–5236, https://doi.org/10.5194/acp-9-5155-2009, 2009.

Hand, J. L., Schichtel, B. A., Pitchford, M., Malm, W. C., and Frank, N. H.: Seasonal composition of remote and urban fine particulate matter in the United States, J. Geophys. Res. Atmospheres, 117, https://doi.org/10.1029/2011JD017122, 2012.

Hidy, G. M., Blanchard, C. L., Baumann, K., Edgerton, E., Tanenbaum, S., Shaw, S., Knipping, E., Tombach, I., Jansen, J., and Walters, J.: Chemical climatology of the southeastern United States, 1999–2013, Atmospheric Chem. Phys., 14, 11893–11914, https://doi.org/10.5194/acp-14-11893-2014, 2014.

Jen, C. N., Hatch, L. E., Selimovic, V., Yokelson, R. J., Weber, R., Fernandez, A. E., Kreisberg, N. M., Barsanti, K. C., and Goldstein, A. H.: Speciated and total emission factors of particulate organics from burning western US wildland fuels and their dependence on combustion efficiency, Atmospheric Chem. Phys., 19, 1013–1026, https://doi.org/10.5194/acp-19-1013-2019, 2019.

550   Kelley, M., Schmidt, G. A., Nazarenko, L. S., Bauer, S. E., Ruedy, R., Russell, G. L., Ackerman, A. S., Aleinov, I.,
551   Bauer, M., Bleck, R., Canuto, V., Cesana, G., Cheng, Y., Clune, T. L., Cook, B. I., Cruz, C. A., Del Genio, A. D.,
552   Elsaesser, G. S., Faluvegi, G., Kiang, N. Y., Kim, D., Lacis, A. A., Leboissetier, A., LeGrande, A. N., Lo, K. K.,
553   Marshall, J., Matthews, E. E., McDermid, S., Mezuman, K., Miller, R. L., Murray, L. T., Oinas, V., Orbe, C.,
554   García-Pando, C. P., Perlwitz, J. P., Puma, M. J., Rind, D., Romanou, A., Shindell, D. T., Sun, S., Tausnev, N.,
555   Tsigaridis, K., Tselioudis, G., Weng, E., Wu, J., and Yao, M.-S.: GISS-E2.1: Configurations and Climatology, J.
556   Adv. Model. Earth Syst., 12, e2019MS002025, https://doi.org/10.1029/2019MS002025, 2020.

557   Kim, P. S., Jacob, D. J., Fisher, J. A., Travis, K., Yu, K., Zhu, L., Yantosca, R. M., Sulprizio, M. P., Jimenez, J. L.,
558   Campuzano-Jost, P., Froyd, K. D., Liao, J., Hair, J. W., Fenn, M. A., Butler, C. F., Wagner, N. L., Gordon, T. D.,
559   Welti, A., Wennberg, P. O., Crounse, J. D., St. Clair, J. M., Teng, A. P., Millet, D. B., Schwarz, J. P., Markovic, M.
560   Z., and Perring, A. E.: Sources, seasonality, and trends of southeast US aerosol: an integrated analysis of surface,
561   aircraft, and satellite observations with the GEOS-Chem chemical transport model, Atmospheric Chem. Phys., 15,
562   10411–10433, https://doi.org/10.5194/acp-15-10411-2015, 2015.

563   Le Breton, M., Wang, Y., Hallquist, Å. M., Pathak, R. K., Zheng, J., Yang, Y., Shang, D., Glasius, M., Bannan, T.
564   J., Liu, Q., Chan, C. K., Percival, C. J., Zhu, W., Lou, S., Topping, D., Wang, Y., Yu, J., Lu, K., Guo, S., Hu, M.,
565   and Hallquist, M.: Online gas- and particle-phase measurements of organosulfates, organosulfonates and nitrooxy
566   organosulfates in Beijing utilizing a FIGAERO ToF-CIMS, Atmospheric Chem. Phys., 18, 10355–10371,
567   https://doi.org/10.5194/acp-18-10355-2018, 2018.

568   Lee, L. A., Reddington, C. L., and Carslaw, K. S.: On the relationship between aerosol model uncertainty and
569   radiative forcing uncertainty, Proc. Natl. Acad. Sci., 113, 5820–5827, https://doi.org/10.1073/pnas.1507050113,
570   2016.

571   Leeper, R. D., Bilotta, R., Petersen, B., Stiles, C. J., Heim, R., Fuchs, B., Prat, O. P., Palecki, M., and Ansari, S.:
572   Characterizing U.S. drought over the past 20 years using the U.S. drought monitor, Int. J. Climatol., 42, 6616–6630,
573   https://doi.org/10.1002/joc.7653, 2022.

574   Li, W. and Wang, Y.: Reduced surface fine dust under droughts over the southeastern United States during
575   summertime: observations and CMIP6 model simulations, Atmospheric Chem. Phys., 22, 7843–7859,
576   https://doi.org/10.5194/acp-22-7843-2022, 2022.

577   Li, W., Wang, Y., Flynn, J., Griffin, R. J., Guo, F., and Schnell, J. L.: Spatial variation of surface O3 responses to
578   drought over the contiguous United States during summertime: Role of precursor emissions and ozone chemistry, J.
579   Geophys. Res. Atmospheres, 127, e2021JD035607, https://doi.org/10.1029/2021JD035607, 2022.

580   Llusià, J., Peñuelas, J., Alessio, G. A., and Estiarte, M.: Contrasting Species-Specific, Compound-Specific,
581   Seasonal, and Interannual Responses of Foliar Isoprenoid Emissions to Experimental Drought in a Mediterranean
582   Shrubland, Int. J. Plant Sci., 169, 637–645, https://doi.org/10.1086/533603, 2008.

583   Lopez-Hilfiker, F. D., Mohr, C., D'Ambro, E. L., Lutz, A., Riedel, T. P., Gaston, C. J., Iyer, S., Zhang, Z., Gold, A.,
584   Surratt, J. D., Lee, B. H., Kurten, T., Hu, W. W., Jimenez, J., Hallquist, M., and Thornton, J. A.: Molecular
585   composition and volatility of organic aerosol in the southeastern U.S.: Implications for IEPOX derived SOA,
586   Environ. Sci. Technol., 50, 2200–2209, https://doi.org/10.1021/acs.est.5b04769, 2016.

587   Malm, W. C., Schichtel, B. A., Hand, J. L., and Collett Jr., J. L.: Concurrent temporal and spatial trends in sulfate
588   and organic mass concentrations measured in the IMPROVE monitoring program, J. Geophys. Res. Atmospheres,
589   122, 10,462-10,476, https://doi.org/10.1002/2017JD026865, 2017.

590   Maria, S. F., Russell, L. M., Gilles, M. K., and Myneni, S. C. B.: Organic Aerosol Growth Mechanisms and Their
591   Climate-Forcing Implications, Science, 306, 1921–1924, https://doi.org/10.1126/science.1103491, 2004.

592   McClure, C. D. and Jaffe, D. A.: US particulate matter air quality improves except in wildfire-prone areas, Proc.
593   Natl. Acad. Sci., 115, 7901–7906, https://doi.org/10.1073/pnas.1804353115, 2018.

594 NASA: CERES Time-Interpolated TOA Fluxes, Clouds and Aerosols Monthly Terra Edition4A, NASA Langley
595 Atmospheric Science Data Center DAAC [data set],
596 https://doi.org/10.5067/TERRA/CERES/SSF1DEGMONTH_L3.004A, 2015.

597 van Noije, T., Bergman, T., Le Sager, P., O'Donnell, D., Makkonen, R., Gonçalves-Ageitos, M., Döscher, R.,
598 Fladrich, U., von Hardenberg, J., Keskinen, J.-P., Korhonen, H., Laakso, A., Myriokefalitakis, S., Ollinaho, P., Pérez
599 García-Pando, C., Reerink, T., Schrödner, R., Wyser, K., and Yang, S.: EC-Earth3-AerChem: a global climate
600 model with interactive aerosols and atmospheric chemistry participating in CMIP6, Geosci. Model Dev., 14, 5637–
601 5668, https://doi.org/10.5194/gmd-14-5637-2021, 2021.

602 Pegoraro, E., Rey, A., Barron-Gafford, G., Monson, R., Malhi, Y., and Murthy, R.: The interacting effects of
603 elevated atmospheric CO_2 concentration, drought and leaf-to-air vapour pressure deficit on ecosystem isoprene
604 fluxes, Oecologia, 146, 120–129, https://doi.org/10.1007/s00442-005-0166-5, 2005.

605 Potosnak, M. J., LeStourgeon, L., Pallardy, S. G., Hosman, K. P., Gu, L., Karl, T., Geron, C., and Guenther, A. B.:
606 Observed and modeled ecosystem isoprene fluxes from an oak-dominated temperate forest and the influence of
607 drought stress, Atmos. Environ., 84, 314–322, https://doi.org/10.1016/j.atmosenv.2013.11.055, 2014.

608 Pye, H. O. T., Murphy, B. N., Xu, L., Ng, N. L., Carlton, A. G., Guo, H., Weber, R., Vasilakos, P., Appel, K. W.,
609 Budisulistiorini, S. H., Surratt, J. D., Nenes, A., Hu, W., Jimenez, J. L., Isaacman-VanWertz, G., Misztal, P. K., and
610 Goldstein, A. H.: On the implications of aerosol liquid water and phase separation for organic aerosol mass,
611 Atmospheric Chem. Phys., 17, 343–369, https://doi.org/10.5194/acp-17-343-2017, 2017.

612 Pye, H. O. T., Ward-Caviness, C. K., Murphy, B. N., Appel, K. W., and Seltzer, K. M.: Secondary organic aerosol
613 association with cardiorespiratory disease mortality in the United States, Nat. Commun., 12, 7215,
614 https://doi.org/10.1038/s41467-021-27484-1, 2021.

615 Randerson, J. T., Chen, Y., van der Werf, G. R., Rogers, B. M., and Morton, D. C.: Global burned area and biomass
616 burning emissions from small fires, J. Geophys. Res. Biogeosciences, 117, https://doi.org/10.1029/2012JG002128,
617 2012.

618 Rasch, P. J., Barth, M. C., Kiehl, J. T., Schwartz, S. E., and Benkovitz, C. M.: A description of the global sulfur
619 cycle and its controlling processes in the National Center for Atmospheric Research Community Climate Model,
620 Version 3, J. Geophys. Res. Atmospheres, 105, 1367–1385, https://doi.org/10.1029/1999JD900777, 2000.

621 Ridley, D. A., Heald, C. L., Ridley, K. J., and Kroll, J. H.: Causes and consequences of decreasing atmospheric
622 organic aerosol in the United States, Proc. Natl. Acad. Sci., 115, 290–295, https://doi.org/10.1073/pnas.1700387115,
623 2018.

624 Riva, M., Tomaz, S., Cui, T., Lin, Y.-H., Perraudin, E., Gold, A., Stone, E. A., Villenave, E., and Surratt, J. D.:
625 Evidence for an Unrecognized Secondary Anthropogenic Source of Organosulfates and Sulfonates: Gas-Phase
626 Oxidation of Polycyclic Aromatic Hydrocarbons in the Presence of Sulfate Aerosol, Environ. Sci. Technol., 49,
627 6654–6664, https://doi.org/10.1021/acs.est.5b00836, 2015.

628 Ruffault, J., Curt, T., Martin-StPaul, N. K., Moron, V., and Trigo, R. M.: Extreme wildfire events are linked to
629 global-change-type droughts in the northern Mediterranean, Nat. Hazards Earth Syst. Sci., 18, 847–856,
630 https://doi.org/10.5194/nhess-18-847-2018, 2018.

631 Scasta, J. D., Weir, J. R., and Stambaugh, M. C.: Droughts and wildfires in western U.S. rangelands, Rangelands,
632 38, 197–203, https://doi.org/10.1016/j.rala.2016.06.003, 2016.

633 Schnell, J. L., Holmes, C. D., Jangam, A., and Prather, M. J.: Skill in forecasting extreme ozone pollution episodes
634 with a global atmospheric chemistry model, Atmospheric Chem. Phys., 14, 7721–7739, https://doi.org/10.5194/acp-
635 14-7721-2014, 2014.

636 Schroder, J. C., Campuzano-Jost, P., Day, D. A., Shah, V., Larson, K., Sommers, J. M., Sullivan, A. P., Campos, T.,
637 Reeves, J. M., Hills, A., Hornbrook, R. S., Blake, N. J., Scheuer, E., Guo, H., Fibiger, D. L., McDuffie, E. E., Hayes,
638 P. L., Weber, R. J., Dibb, J. E., Apel, E. C., Jaeglé, L., Brown, S. S., Thornton, J. A., and Jimenez, J. L.: Sources and
639 secondary production of organic aerosols in the northeastern United States during winter, J. Geophys. Res.
640 Atmospheres, 123, 7771–7796, https://doi.org/10.1029/2018JD028475, 2018.

641 Séférian, R., Nabat, P., Michou, M., Saint-Martin, D., Voldoire, A., Colin, J., Decharme, B., Delire, C., Berthet, S.,
642 Chevallier, M., Sénési, S., Franchisteguy, L., Vial, J., Mallet, M., Joetzjer, E., Geoffroy, O., Guérémy, J.-F., Moine,
643 M.-P., Msadek, R., Ribes, A., Rocher, M., Roehrig, R., Salas-y-Mélia, D., Sanchez, E., Terray, L., Valcke, S.,
644 Waldman, R., Aumont, O., Bopp, L., Deshayes, J., Éthé, C., and Madec, G.: Evaluation of CNRM Earth System
645 Model, CNRM-ESM2-1: Role of Earth System Processes in Present-Day and Future Climate, J. Adv. Model. Earth
646 Syst., 11, 4182–4227, https://doi.org/10.1029/2019MS001791, 2019.

647 Seland, Ø., Bentsen, M., Olivié, D., Toniazzo, T., Gjermundsen, A., Graff, L. S., Debernard, J. B., Gupta, A. K., He,
648 Y.-C., Kirkevåg, A., Schwinger, J., Tjiputra, J., Aas, K. S., Bethke, I., Fan, Y., Griesfeller, J., Grini, A., Guo, C.,
649 Ilicak, M., Karset, I. H. H., Landgren, O., Liakka, J., Moseid, K. O., Nummelin, A., Spensberger, C., Tang, H.,
650 Zhang, Z., Heinze, C., Iversen, T., and Schulz, M.: Overview of the Norwegian Earth System Model (NorESM2)
651 and key climate response of CMIP6 DECK, historical, and scenario simulations, Geosci. Model Dev., 13, 6165–
652 6200, https://doi.org/10.5194/gmd-13-6165-2020, 2020.

653 Senior, C. A., Jones, C. G., Wood, R. A., Sellar, A., Belcher, S., Klein-Tank, A., Sutton, R., Walton, J., Lawrence,
654 B., Andrews, T., and Mulcahy, J. P.: U.K. Community Earth System Modeling for CMIP6, J. Adv. Model. Earth
655 Syst., 12, e2019MS002004, https://doi.org/10.1029/2019MS002004, 2020.

656 Shrivastava, M., Cappa, C. D., Fan, J., Goldstein, A. H., Guenther, A. B., Jimenez, J. L., Kuang, C., Laskin, A.,
657 Martin, S. T., Ng, N. L., Petaja, T., Pierce, J. R., Rasch, P. J., Roldin, P., Seinfeld, J. H., Shilling, J., Smith, J. N.,
658 Thornton, J. A., Volkamer, R., Wang, J., Worsnop, D. R., Zaveri, R. A., Zelenyuk, A., and Zhang, Q.: Recent
659 advances in understanding secondary organic aerosol: Implications for global climate forcing, Rev. Geophys., 55,
660 509–559, https://doi.org/10.1002/2016RG000540, 2017.

661 Strzepek, K., Yohe, G., Neumann, J., and Boehlert, B.: Characterizing changes in drought risk for the United States
662 from climate change, Environ. Res. Lett., 5, 044012, https://doi.org/10.1088/1748-9326/5/4/044012, 2010.

663 Surratt, J. D., Chan, A. W. H., Eddingsaas, N. C., Chan, M., Loza, C. L., Kwan, A. J., Hersey, S. P., Flagan, R. C.,
664 Wennberg, P. O., and Seinfeld, J. H.: Reactive intermediates revealed in secondary organic aerosol formation from
665 isoprene, Proc. Natl. Acad. Sci., 107, 6640–6645, https://doi.org/10.1073/pnas.0911114107, 2010.

666 Tai, A. P. K., Mickley, L. J., and Jacob, D. J.: Correlations between fine particulate matter (PM2.5) and
667 meteorological variables in the United States: Implications for the sensitivity of PM2.5 to climate change, Atmos.
668 Environ., 44, 3976–3984, https://doi.org/10.1016/j.atmosenv.2010.06.060, 2010.

669 Tatebe, H., Ogura, T., Nitta, T., Komuro, Y., Ogochi, K., Takemura, T., Sudo, K., Sekiguchi, M., Abe, M., Saito, F.,
670 Chikira, M., Watanabe, S., Mori, M., Hirota, N., Kawatani, Y., Mochizuki, T., Yoshimura, K., Takata, K., O'ishi,
671 R., Yamazaki, D., Suzuki, T., Kurogi, M., Kataoka, T., Watanabe, M., and Kimoto, M.: Description and basic
672 evaluation of simulated mean state, internal variability, and climate sensitivity in MIROC6, Geosci. Model Dev., 12,
673 2727–2765, https://doi.org/10.5194/gmd-12-2727-2019, 2019.

674 Taufik, M., Torfs, P. J. J. F., Uijlenhoet, R., Jones, P. D., Murdiyarso, D., and Van Lanen, H. A. J.: Amplification of
675 wildfire area burnt by hydrological drought in the humid tropics, Nat. Clim. Change, 7, 428–431,
676 https://doi.org/10.1038/nclimate3280, 2017.

677 Thornhill, G., Collins, W., Olivié, D., Skeie, R. B., Archibald, A., Bauer, S., Checa-Garcia, R., Fiedler, S., Folberth,
678 G., Gjermundsen, A., Horowitz, L., Lamarque, J.-F., Michou, M., Mulcahy, J., Nabat, P., Naik, V., O'Connor, F.
679 M., Paulot, F., Schulz, M., Scott, C. E., Séférian, R., Smith, C., Takemura, T., Tilmes, S., Tsigaridis, K., and Weber,

680   J.: Climate-driven chemistry and aerosol feedbacks in CMIP6 Earth system models, Atmospheric Chem. Phys., 21,
681   1105–1126, https://doi.org/10.5194/acp-21-1105-2021, 2021.

682   Tsui, W. G., Woo, J. L., and McNeill, V. F.: Impact of Aerosol-Cloud Cycling on Aqueous Secondary Organic
683   Aerosol Formation, Atmosphere, 10, 666, https://doi.org/10.3390/atmos10110666, 2019.

684   Turnock, S. T., Allen, R. J., Andrews, M., Bauer, S. E., Deushi, M., Emmons, L., Good, P., Horowitz, L., John, J.
685   G., Michou, M., Nabat, P., Naik, V., Neubauer, D., O'Connor, F. M., Olivié, D., Oshima, N., Schulz, M., Sellar, A.,
686   Shim, S., Takemura, T., Tilmes, S., Tsigaridis, K., Wu, T., and Zhang, J.: Historical and future changes in air
687   pollutants from CMIP6 models, Atmospheric Chem. Phys., 20, 14547–14579, https://doi.org/10.5194/acp-20-
688   14547-2020, 2020.

689   Vicente-Serrano, S. M., Beguería, S., and López-Moreno, J. I.: A multiscalar drought index sensitive to global
690   warming: The Standardized Precipitation Evapotranspiration Index, J. Clim., 23, 1696–1718,
691   https://doi.org/10.1175/2009JCLI2909.1, 2010.

692   Wang, Y., Xie, Y., Cai, L., Dong, W., Zhang, Q., and Zhang, L.: Impact of the 2011 southern U.S. drought on
693   ground-level fine aerosol concentration in summertime, J. Atmospheric Sci., 72, 1075–1093,
694   https://doi.org/10.1175/JAS-D-14-0197.1, 2015.

695   Wang, Y., Xie, Y., Dong, W., Ming, Y., Wang, J., and Shen, L.: Adverse effects of increasing drought on air quality
696   via natural processes, Atmospheric Chem. Phys., 17, 12827–12843, https://doi.org/10.5194/acp-17-12827-2017,
697   2017.

698   Wang, Y., Wang, J., Wang, Y., and Li, W.: Drought impacts on PM2.5 composition and amount over the US during
699   1988–2018, J. Geophys. Res. Atmospheres, 127, e2022JD037677, https://doi.org/10.1029/2022JD037677, 2022a.

700   Wang, Y., Lin, N., Li, W., Guenther, A., Lam, J. C. Y., Tai, A. P. K., Potosnak, M. J., and Seco, R.: Satellite-
701   derived constraints on the effect of drought stress on biogenic isoprene emissions in the southeastern US,
702   Atmospheric Chem. Phys., 22, 14189–14208, https://doi.org/10.5194/acp-22-14189-2022, 2022b.

703   Wilhite, D. A., Svoboda, M. D., and Hayes, M. J.: Understanding the complex impacts of drought: A key to
704   enhancing drought mitigation and preparedness, Water Resour. Manag., 21, 763–774,
705   https://doi.org/10.1007/s11269-006-9076-5, 2007.

706   Wu, C., Pullinen, I., Andres, S., Carriero, G., Fares, S., Goldbach, H., Hacker, L., Kasal, T., Kiendler-Scharr, A.,
707   Kleist, E., Paoletti, E., Wahner, A., Wildt, J., and Mentel, T. F.: Impacts of soil moisture on de novo monoterpene
708   emissions from European beech, Holm oak, Scots pine, and Norway spruce, Biogeosciences, 12, 177–191,
709   https://doi.org/10.5194/bg-12-177-2015, 2015.

710   Wu, T., Zhang, F., Zhang, J., Jie, W., Zhang, Y., Wu, F., Li, L., Yan, J., Liu, X., Lu, X., Tan, H., Zhang, L., Wang,
711   J., and Hu, A.: Beijing Climate Center Earth System Model version 1 (BCC-ESM1): model description and
712   evaluation of aerosol simulations, Geosci. Model Dev., 13, 977–1005, https://doi.org/10.5194/gmd-13-977-2020,
713   2020.

714   Xie, Y., Wang, Y., Dong, W., Wright, J. S., Shen, L., and Zhao, Z.: Evaluating the response of summertime surface
715   sulfate to hydroclimate variations in the continental United States: Role of meteorological inputs in the GEOS-Chem
716   model, J. Geophys. Res. Atmospheres, 124, 1662–1679, https://doi.org/10.1029/2018JD029693, 2019.

717   Xu, L., Guo, H., Boyd, C. M., Klein, M., Bougiatioti, A., Cerully, K. M., Hite, J. R., Isaacman-VanWertz, G.,
718   Kreisberg, N. M., and Knote, C.: Effects of anthropogenic emissions on aerosol formation from isoprene and
719   monoterpenes in the southeastern United States, Proc. Natl. Acad. Sci., 112, 37–42, 2015.

720   Yli-Juuti, T., Mielonen, T., Heikkinen, L., Arola, A., Ehn, M., Isokääntä, S., Keskinen, H.-M., Kulmala, M., Laakso,
721   A., Lipponen, A., Luoma, K., Mikkonen, S., Nieminen, T., Paasonen, P., Petäjä, T., Romakkaniemi, S., Tonttila, J.,

722   Kokkola, H., and Virtanen, A.: Significance of the organic aerosol driven climate feedback in the boreal area, Nat.
723   Commun., 12, 5637, https://doi.org/10.1038/s41467-021-25850-7, 2021.

724   Yukimoto, S., Kawai, H., Koshiro, T., Oshima, N., Yoshida, K., Urakawa, S., Tsujino, H., Deushi, M., Tanaka, T.,
725   Hosaka, M., Yabu, S., Yoshimura, H., Shindo, E., Mizuta, R., Obata, A., Adachi, Y., and Ishii, M.: The
726   Meteorological Research Institute Earth System Model Version 2.0, MRI-ESM2.0: Description and Basic
727   Evaluation of the Physical Component, J. Meteorol. Soc. Jpn. Ser II, 97, 931–965,
728   https://doi.org/10.2151/jmsj.2019-051, 2019.

729   Zhang, Q., Jimenez, J. L., Canagaratna, M. R., Ulbrich, I. M., Ng, N. L., Worsnop, D. R., and Sun, Y.:
730   Understanding atmospheric organic aerosols via factor analysis of aerosol mass spectrometry: a review, Anal.
731   Bioanal. Chem., 401, 3045–3067, https://doi.org/10.1007/s00216-011-5355-y, 2011.

732   Zhang, X., Liu, Z., Hecobian, A., Zheng, M., Frank, N. H., Edgerton, E. S., and Weber, R. J.: Spatial and seasonal
733   variations of fine particle water-soluble organic carbon (WSOC) over the southeastern United States: implications
734   for secondary organic aerosol formation, Atmospheric Chem. Phys., 12, 6593–6607, https://doi.org/10.5194/acp-12-
735   6593-2012, 2012.

736   Zhao, Z., Wang, Y., Qin, M., Hu, Y., Xie, Y., and Russell, A. G.: Drought impacts on secondary organic aerosol: a
737   case study in the southeast United States, Environ. Sci. Technol., 53, 242–250,
738   https://doi.org/10.1021/acs.est.8b04842, 2019.

739   Zheng, Y., Thornton, J. A., Ng, N. L., Cao, H., Henze, D. K., McDuffie, E. E., Hu, W., Jimenez, J. L., Marais, E. A.,
740   Edgerton, E., and Mao, J.: Long-term observational constraints of organic aerosol dependence on inorganic species
741   in the southeast US, Atmospheric Chem. Phys., 20, 13091–13107, https://doi.org/10.5194/acp-20-13091-2020,
742   2020.

743
744